Polarizable contributions to the surface tension of liquid water

Jose L. Rivera[a)]
Department of Physics, Wesleyan University, Middletown, Connecticut 06459
and Department of Chemical Engineering, Universidad Michoacana de San Nicolás de Hidalgo, Morelia, Michoacán, 58000, México

Francis W. Starr
Department of Physics, Wesleyan University, Middletown, Connecticut 06459

Patrice Paricaud
Laboratoire de Chimie et Procédés, École Nationale Superiéure de Techniques Avancées (ENSTA), 75739 Paris Cedex 15, France

Peter T. Cummings
Department of Chemical Engineering, Vanderbilt University, Nashville, Tennessee 37235
and Chemical Sciences Division, Oak Ridge National Laboratory, Oak Ridge, Tennessee 37831

(Received 8 May 2006; accepted 1 August 2006; published online 5 September 2006)

Surface tension, γ, strongly affects interfacial properties in fluids. The degree to which polarizability affects γ in water is thus far not well established. To address this situation, we carry out molecular dynamics simulations to study the interfacial forces acting on a slab of liquid water surrounded by vacuum using the Gaussian charge polarizable (GCP) model at 298.15 K. The GCP model incorporates both a fixed dipole due to Gaussian distributed charges and a polarizable dipole. We find a well-defined bulklike region forms with a width of $\approx$31 Å. The average density of the bulklike region agrees with the experimental value of 0.997 g/cm^3. However, we find that the orientation of the molecules in the bulklike region is strongly influenced by the interfaces, even at a distance five molecular diameters from the interface. Specifically, the orientations of both the permanent and induced dipoles show a preferred orientation parallel to the interface. Near the interface, the preferred orientation of the dipoles becomes more pronounced and the average magnitude of the induced dipoles decreases monotonically. To quantify the degree to which molecular orientation affects γ, we calculate the contributions to γ from permanent dipolar interactions, induced dipolar interactions, and dispersion forces. We find that the induced dipole interactions and the permanent dipole interactions, as well as the cross interactions, have positive contributions to γ, and therefore contribute stability to the interface. The repulsive core interactions result in a negative contribution to γ, which nearly cancels the positive contributions from the dipoles. The large negative core contributions to γ are the result of small oxygen-oxygen separation between molecules. These small separations occur due to the strong attractions between hydrogen and oxygen atoms. The final predicted value for γ (68.65 mN/m) shows a deviation of $\approx$4% of the experimental value of 71.972 mN/m. The inclusion of polarization is critical for this model to produce an accurate value. © *2006 American Institute of Physics*. [DOI: 10.1063/1.2345063]

I. INTRODUCTION

Phase equilibrium and nonequilibrium thermodynamic phenomena involving water and its mixtures are fundamental to study many chemical, biological, and mineralogical systems, and therefore its understanding is essential to improve many technological and industrial applications.[1–3] Interfaces are particularly important in these phenomena, since in the interfacial regions, momentum, mass, and heat are exchanged with the surroundings to reach phase equilibrium, which is characterized by macroscopic properties, such as the surface tension, γ.[4,5] Interfaces are difficult to characterize since, even if the properties in the bulk region are known, the small thickness of the interfacial region (on the order of angstroms) requires complex experimental techniques. For example, x-ray scattering measurements can be used to estimate the interfacial thickness, and indirectly produce a profile of the normalized electron density.[6,7]

Given the experimental complications associated with interfacial studies, it makes sense to complement experimental approaches with computational studies. Since the molecular properties may be very sensitive to the distance from the interface, it is important to account for the possibility that the charge distribution of the molecules may be different near the interface. Polarizable models of water which can capture variability of the charge distribution have been used extensively to study the saturated bulk properties of water, including saturated densities, vapor pressure, and vaporization en-

[a)]Author to whom correspondence should be addressed. Electronic mail: rivera_jose_l@yahoo.com

thalpy in the vapor-liquid and liquid-liquid equilibria using the Gibbs ensemble Monte Carlo[8–11] (GEMC) and molecular dynamics (MD) methodologies.[8,9]

The liquid-vapor interface was studied via MD methodology by Motakabbir and Berkowitz[12] using a polarizable model of water with four interaction sites. They found that the inclusion of polarizability does not contribute significantly to the prediction of the structural and orientation properties of molecules near the interface. They also found that the fixed molecular dipole orientation is roughly parallel to the interface. Both the magnitude of the induced dipoles, and the coupling between induced and permanent dipole orientation decreases monotonically moving toward the interface.

More recently, the hydrogen-bond dynamics at the air-liquid interface of water was studied by Liu *et al.*[13] using the polarizable TIP4P/FQ model at 1 atm and 298.15 K. They found that hydrogen bonds at the interface form and break faster than hydrogen bonds in the bulk phase and that this behavior produces an increase in the diffusion coefficient in the interfacial region relative to the bulk. They explained this behavior as a result of a decrease in the number of hydrogen bonded molecules at the interface.

In a previous work, we reported the calculations of γ for the self-consistent point-dipole polarizable model of water for several temperatures in the vapor-liquid region.[8] Those calculations provided an overall average γ, but they did not provide information about the contributions to γ due to each specific molecular interaction in the polarizable model as a function of the position relative to the interface. The previous simulations demonstrated that the contribution of the polarizability to the structural and orientation properties is not significant, but the contribution of the polarizability to the surface forces was not evaluated.

In this work we study the contributions to γ using MD calculations. We find that polarizability contributes roughly one third of the total positive contributions to γ. We also find that most of the dipoles are orientated parallel to the interface, even in the bulklike region. The paper is arranged as follows: In Sec. II we described the potential model and the methodology employed in this work. Section III ontains the results for the contributions to γ and a discussion of the ordering of the molecules at the bulk and interfacial regions and their influence on γ. The conclusions of this work are presented in Sec. IV.

II. POTENTIAL MODEL AND METHODOLOGY

The Gaussian charge polarizable model of water, developed by Paricaud al.[9] consists of three Gaussian distributed charges. The Gaussian distributed charges result in a permanent dipole of 1.855 D, which corresponds to the experimental value of an isolated water molecule.[14] Additionally, the model includes a polarizable dipole at the molecule's center of mass. The molecular geometry is the same as the experimental gas phase geometry[15] with an O–H distance of 0.9572 Å and a H–O–H angle of 104.52°. The positive Gaussian distributed charges are located at the hydrogen atoms while the negative charge, M, is located at the bisector of the angle H–O–H at a distance of 0.27 Å away from the oxygen. The dispersion interactions are accounted with an exponential repulsive core and a $1/r^6$ attractive tail between the oxygen atoms. We refer to this combined interaction as an exp-6 interaction,

$$U_{\text{exp-6}} = \frac{1}{2}\sum_{j\neq i}^{N} \frac{\varepsilon}{1-6/\gamma}\left(\frac{6}{\gamma}\exp\left(\gamma\left[1-\frac{r_{i4j4}}{\sigma}\right]\right)-\left(\frac{\sigma}{r_{i4j4}}\right)^6\right), \tag{1}$$

where N is the number of molecules, r_{i4j4} is the oxygen-oxygen distance between molecules i and j, $\varepsilon/k_B=110$ K, k_B is the Boltzman's constant, $\sigma=3.69$ Å, and $\gamma=12.75$.

Permanent dipole-permanent dipole potential energy is calculated through its permanent Gaussian distributed charge-charge potential,

$$U_{qq} = \frac{1}{2}\sum_{j\neq i}^{N}\sum_{a=1}^{3}\sum_{b=1}^{3}\frac{q_a q_b}{4\pi\varepsilon_0 r_{iajb}}\operatorname{erf}\left(\frac{r_{iajb}}{\sqrt{2(\sigma_a^2+\sigma_b^2)}}\right), \tag{2}$$

where r_{iajb} is the distance between force site a in molecule i and force site b in molecule j. Sites 1–3 correspond to the Gaussian distributed charges hydrogen 1, hydrogen 2, and M, respectively. $q_1=q_2=0.6113e$, $q_3=-2q_1$, ε_0 is the permittivity of vacuum, $\sigma_1=\sigma_2=0.455$ Å, $\sigma_3=0.610$ Å, and erf is the error function. The induced dipole $\mathbf{p}_i$ is proportional to the total electric field at the center of mass of molecule i and is given by

$$\mathbf{p}_i = \alpha_{\text{pol}}(\mathbf{E}_i^q + \mathbf{E}_i^p), \tag{3}$$

where $\alpha_{\text{pol}}=1.444$ Å^3 is the experimental molecular polarization of water. $\mathbf{E}_i^q$ and $\mathbf{E}_i^p$ are the electric fields at the center of mass of molecule i due to the Gaussian distributed charges and induced dipoles, $\mathbf{p}_j$, of molecules $j\neq i$. $\mathbf{E}_i^q$ is given by

$$\mathbf{E}_i^q = \sum_{j\neq i}^{N}\sum_{b=1}^{3}\frac{q_b(\mathbf{r}_i-\mathbf{r}_{jb})}{4\pi\varepsilon_0 r_{ijb}^3}\left[\operatorname{erf}\left(\frac{r_{ijb}}{\sqrt{2(\sigma_3^2+\sigma_b^2)}}\right)-\frac{\sqrt{2}r_{ijb}}{\sqrt{\pi(\sigma_3^2+\sigma_b^2)}}\exp\left(\frac{-r_{ijb}^2}{2(\sigma_3^2+\sigma_b^2)}\right)\right], \tag{4}$$

where r_{ijb} is the distance between the center of mass of molecule i and force site b in molecule j. $\mathbf{r}_i$ and $\mathbf{r}_{jb}$ are the position vectors of the center of mass of molecule i and force site b in molecule j, respectively. $\mathbf{E}_i^p$ is given by

$$\mathbf{E}_i^p = \sum_{j\neq i}^{N}\frac{1}{r_{ij}^3}\left[\left(f\frac{3\mathbf{r}_{ij}\mathbf{r}_{ij}}{r_{ij}^2}-g\mathbf{I}\right)\cdot\mathbf{p}_j\right], \tag{5}$$

where $r_{ij}=|\mathbf{r}_i-\mathbf{r}_j|$, $\mathbf{I}$ is the 3×3 unit matrix, and $\mathbf{r}_{ij}\mathbf{r}_{ij}$ is the 3×3 vector direct product of $\mathbf{r}_{ij}$. f and g are scalars given by

$$f = \operatorname{erf}\left(\frac{r_{ij}}{2\sigma_3}\right)-\left[\frac{r_{ij}}{\sqrt{\pi}\sigma_3}+\frac{r_{ij}^3}{6\sqrt{\pi}\sigma_3^3}\right]\exp\left(\frac{-r_{ij}^2}{4\sigma_3^2}\right),$$

$$g = \operatorname{erf}\left(\frac{r_{ij}}{2\sigma_3}\right)-\frac{r_{ij}}{\sqrt{\pi}\sigma_3}\exp\left(\frac{-r_{ij}^2}{4\sigma_3^2}\right). \tag{6}$$

Equations (3) and (5) are solved by iteration of the induced dipoles $\mathbf{p}_j$. Permanent-induced and induced-induced dipoles potential energies are then calculated by

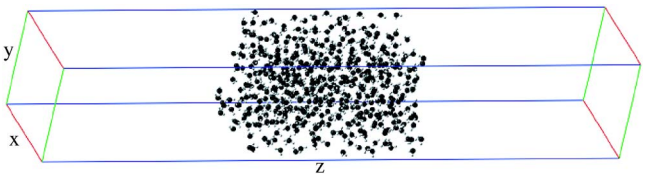

FIG. 1. Snapshot of the simulated system: A slab of liquid water formed by 500 molecules is surrounded by vacuum at 298.15 K. The parallelepiped represents the actual size of the simulation cell.

$$U_{qI} = -\sum_{i=1}^{N} \mathbf{p}_i \cdot \mathbf{E}_i^q, \tag{7}$$

$$U_{II} = -\frac{1}{2}\sum_{i=1}^{N} \mathbf{p}_i \cdot \mathbf{E}_i^p + \frac{1}{2\alpha_{\text{pol}}}\sum_{i=1}^{N} \mathbf{p}_i^2. \tag{8}$$

Explicit interactions are truncated at a cutoff radius of 9 Å. We calculate long-range electrostatic corrections using the reaction-field method.[16] The GCM model has been used to calculate the vapor-liquid equilibrium, including predictions of the saturated densities, vapor pressures, dielectric constant of saturated liquid, and the enthalpy of vaporization, and produces excellent agreement with experimental data even for temperatures as close to the critical point as 32 K.

We use the MD methodology to simulate the vacuum-liquid equilibrium (VLE) of water at 298.15 K. This methodology has been employed in previous works to study the bulk and interfacial properties of systems in vapor-liquid equilibrium, including polar,[17–19] nonpolar,[20] and their mixtures.[21–23] We integrate the equations of motion using the Gear fourth-order predictor-corrector algorithm with a time step of 1 fs, and control the temperature using the Gaussian isokinetic thermostat[24,25] and the Evans-Murad quaternion formalism.[26] The initial system consists of a cubic cell of water molecules surrounded by two empty rectangular cells. The dimensions of the combined simulation cell are $21\times21\times126$ Å^3, and the cell contains 500 molecules of water. We use 600 000 configurations (600 ps) to generate statistical averages of the properties, following an initial run of 400 ps for equilibration. A previous work with a polarizable model of water found that the relaxation times for water at the bulk and at the interface are 4.93 and 4.07 ps, respectively.[13] To equilibrate, the system was slowly heated, starting from a configuration at 0 K, in order to avoid translation of the "slab" of water through the simulation cell. An illustrative snapshot of the system is shown in Fig. 1.

We calculate γ from the components of the pressure tensor,

$$\gamma = \int_{-\infty}^{0} [P_N(z) - P_T(z)]dz, \tag{9}$$

where z is the position perpendicular to the interface and the limits of integration take into account only the left interface. The system's center of mass is located at $z=0$. $P_N(z)$ and $P_T(z)$ are the normal and tangential pressure profiles, respectively. We calculate $P_N(z)$ during the simulation via the normal microscopic definition,

$$P_N(z) = \langle\rho(z)\rangle k_B T - \frac{1}{A}\langle[P_{N,1}(z) + P_{N,2}(z) + P_{N,3}(z) + P_{N,4}(z) + P_{N,5}(z)]\rangle, \tag{10}$$

$$P_{N,1}(z) = \sum_{j>i}^{N} \frac{z_{ij}z_{i4j4}}{r_{i4j4}} \frac{dU_{\text{exp-6}}(r_{i4j4})}{dr_{i4j4}} \times \frac{1}{|z_{ij}|} H\left(\frac{z-z_i}{z_{ij}}\right) H\left(\frac{z_j-z}{z_{ij}}\right), \tag{11}$$

$$P_{N,2}(z) = \sum_{j>i}^{N}\sum_{a}^{3}\sum_{b}^{3} \frac{z_{ij}z_{iajb}}{r_{iajb}} \times \frac{dU_{qq}(r_{iajb})}{dr_{iajb}} \frac{1}{|z_{ij}|} H\left(\frac{z-z_i}{z_{ij}}\right) H\left(\frac{z_j-z}{z_{ij}}\right), \tag{12}$$

$$P_{N,3}(z) = \sum_{j\neq i}^{N}\sum_{a}^{3} \frac{z_{ij}z_{iaj}}{r_{iaj}} \frac{dU_{qI}(r_{iaj})}{dr_{iaj}} \frac{1}{|z_{ij}|} H\left(\frac{z-z_i}{z_{ij}}\right) H\left(\frac{z_j-z}{z_{ij}}\right), \tag{13}$$

$$P_{N,4}(z) = \sum_{j\neq i}^{N}\sum_{b}^{3} \frac{z_{ij}z_{ijb}}{r_{ijb}} \frac{dU_{qI}(r_{ijb})}{dr_{ijb}} \frac{1}{|z_{ij}|} H\left(\frac{z-z_i}{z_{ij}}\right) H\left(\frac{z_j-z}{z_{ij}}\right), \tag{14}$$

and

$$P_{N,5}(z) = \sum_{j>i}^{N} \frac{z_{ij}^2}{r_{ij}} \frac{dU_{II}(r_{ij})}{dr_{ij}} \frac{1}{|z_{ij}|} H\left(\frac{z-z_i}{z_{ij}}\right) H\left(\frac{z_j-z}{z_{ij}}\right), \tag{15}$$

where H is the Heaviside function, $\rho(z)$ the density profile, T is the temperature, and A the interfacial area. z_i is the position of the center of mass of molecule i in the z direction. z_{ia} is the position of the ath force site of the ith molecule. We further define $z_{ij}=z_i-z_j$, $z_{iaj}=z_{ia}-z_j$, and $z_{iajb}=z_{ia}-z_{jb}$. r_{iaj} is the distance between force site a in molecule i and the center of mass of molecule j. Equivalent forms of Eqs. (10)–(15) were used to calculate $P_T(z)$, where the terms $z_{ij}z_{i4j4}$, $z_{ij}z_{iajb}$, $z_{ij}z_{iaj}$, $z_{ij}z_{ijb}$, and z_{ij}^2 are replaced by $(x_{ij}x_{i4j4}+y_{ij}y_{i4j4})/2$, $(x_{ij}x_{iajb}+y_{ij}y_{iajb})/2$, $(x_{ij}x_{iaj}+y_{ij}y_{iaj})/2$, $(x_{ij}x_{ijb}+y_{ij}y_{ijb})/2$, and $(x_{ij}^2+y_{ij}^2)/2$ in Eqs. (11)–(15), respectively.

Long range corrections to γ were calculated with the standard expression[27]

$$\gamma_{lrc} = \frac{\pi}{2}\rho_l^2 \int_0^1 ds \int_{r_C}^{\infty} dr_{ij} \coth\left(\frac{r_{ij}s}{d}\right) \frac{dU_{\text{exp-6}}(r_{ij})}{dr_{ij}} \times r_{ij}^4(3s^3 - s), \tag{16}$$

where ρ_l is the average liquid density and r_C is the cutoff radius. d characterizes the interfacial thickness, obtained by fitting the average density profile of the left interface,

$$\rho(z) = \frac{\rho_l}{2}\left[1 + \tanh\left(\frac{z-z_0}{d}\right)\right], \tag{17}$$

where ρ_l is another fitting parameter and z_0 is the position of the Gibbs' dividing surface.

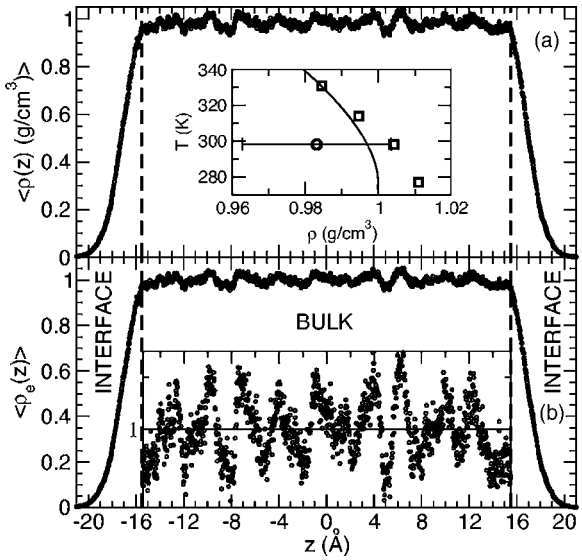

FIG. 2. (a) The average density profile $\langle\rho(z)\rangle$ as a function of the position of the slab in the simulation cell. The inset of the graph shows the temperature-density diagram for saturated liquid water. The circle represents the result of this work, while the squares are the results using GEMC methodology (Ref. 9) and the continuous line is the experimental result (Ref. 35). (b) The normalized average electronic density profile, $\langle\rho_e(z)\rangle$, of water as a function of the position of the slab in the simulation cell. Inside graph is a zoomed view of the bulklike region. The dotted lines roughly demarcate the interfacial region.

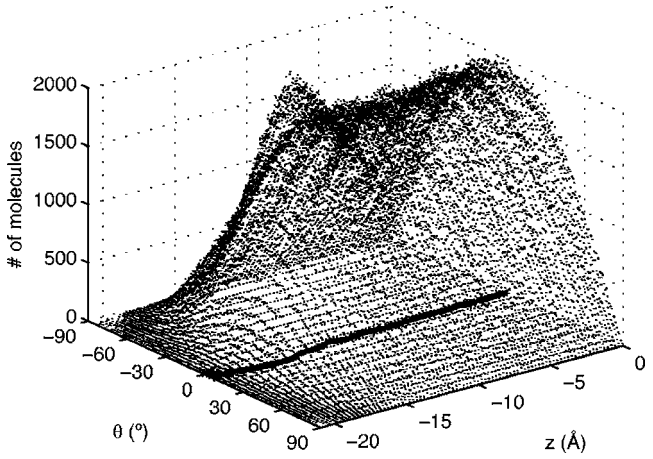

FIG. 3. Histograms of the orientation of the permanent dipole of water as a function of the distance from the center of the slab. The figure shows the left interface up to the center of the bulklike region. The heavy line shows the mean angle as a function of z.

III. RESULTS AND DISCUSSION

A. Density and molecular orientation

To characterize the elementary properties of our system, we first evaluate the density profile perpendicular to the interface. We use a large region of vacuum (compared to the volume of liquid phase) to ensure that molecules at the interfaces do not interact (Fig. 1). The position in the z axis was discretized in N slabs of thickness 0.21 Å. The slab thickness used in this work was optimized as the maximum thickness, which produces reliable statistics for the density profile at the interfacial region. The average density profile $\langle\rho(z)\rangle$ (where z is the position of the center of the slab) from this simulation is shown in Fig. 2(a); from this profile we can see that there is bulklike liquid water with nearly constant density spanning ≈31 Å (≈ nine molecular layers), and interfacial regions at either end spanning ≈5 Å. As previous simulations reported,[8,9] the average density profile of water has a well-defined interfacial region where $\langle\rho(z)\rangle$ decreases and there are no water molecules adsorbed at this interface. We fit Eq. (17) to $\langle\rho(z)\rangle$ and calculate the mean liquid density ρ_l and its standard deviation in the bulklike region $-15.5\ \text{Å} \leqslant z \leqslant 15.5\ \text{Å}$, and find $\rho_l = 0.983 \pm 0.020\ \text{g/cm}^3$; this mean value agrees well with the experimental data for density at $P=1$ atm [inset of Fig. 2(a)]. For comparison, the computed values of ρ_l using the GEMC methodology[9] for the same model are also reported; both methodologies produced results that agree within error. The difference between both values may be due to finite size effects that are important in the simulation of VLE interfaces.

We evaluate the interfacial thickness, d, using Eq. (17). The "10-90 thickness," t, is defined by the distance between the points where $\langle\rho(z)\rangle$ is at 10% and 90% of ρ_l and is related to d by $t=2.1972d$, producing a value of $t \approx 2.9$ Å. This has a relative error of 12% compared to the experimental data.[7] The measured experimental thickness was estimated as the root-mean-square roughness of the interface using x-ray scattering experiments.

We show the normalized average electronic density profile, $\langle\rho_e(z)\rangle$, in Fig. 2(b), defined by the number density of electrons. We normalize $\langle\rho_e(z)\rangle$ by the value in the bulklike region so that $\langle\rho_e(z)\rangle = 1$ in that region. We also show a zoomed view of the bulklike liquid in the inset. The profile of $\langle\rho_e(z)\rangle$ at the interface shows the same qualitative behavior as $\langle\rho(z)\rangle$ from Fig. 2(a). This is not surprising since the electronic density must be closely correlated to the molecular positions. $\langle\rho_e(z)\rangle$ shows nine oscillations in the bulklike liquid region, with variations in the peaks value of ≈0.08. These peaks reflect the mean molecular positions and likely give rise to a mobility dependence with the position in the slab, in agreement with a previous report of low diffusion coefficients found in the bulk water compared to the values found at the interface, reported by Liu *et al.*[13] If we consider that the peaks extend across ≈29 Å, each peak has an average width of ≈3.2 Å, which corresponds to the approximate molecular diameter of water, which has been estimated from adsorption studies of water molecules in micropores.[28]

To obtain information about the orientation of the permanent and induced dipoles, we calculate the angle θ between the dipole direction and the parallel to the interface. Hence $\theta=0$ implies the orientation is parallel to the interface. Figures 3 and 4 show the distributions of angles as a function of the position of the slab. Both distributions show the same qualitative behavior. The distributions are unchanged from the center of the bulklike region up to $z \approx -12$ Å. The peak of these distributions is located at 0°, therefore the preferred orientation of the dipoles in this region is parallel to the interface. The distribution decreases roughly parabolically and vanishes at the perpendicular limits $\theta = \pm 90°$. The fact that in the bulklike region, the distributions are not flat is an indication that this region is not truly bulklike, and that the

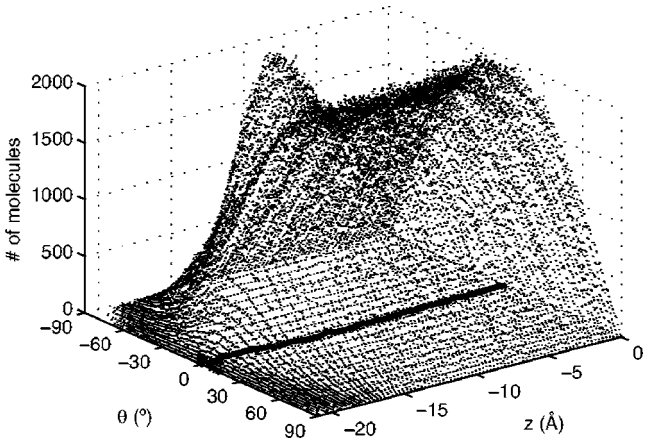

FIG. 4. Histograms of the orientation of the induced dipole of water as a function of the distance from the center of the slab. The figure shows the left interface up to the center of the bulklike region. The heavy line shows the mean angle as a function of z.

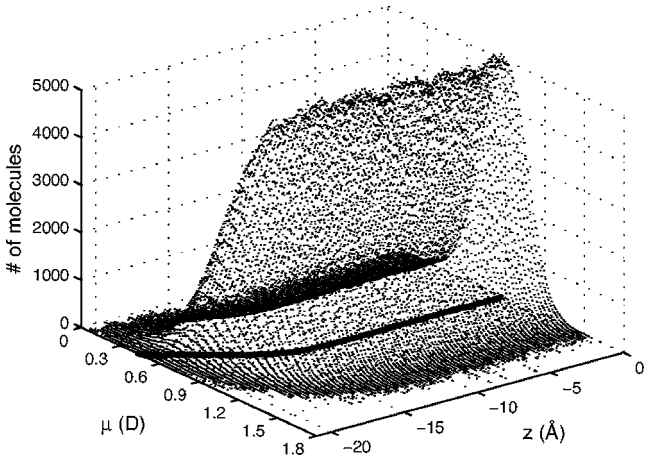

FIG. 5. Histograms of the magnitude of the induced dipole, μ, of water as a function of the distance from the center of the slab. The figure shows the left interface up to the center of the bulklike region. The heavy line shows the mean induced dipole as a function of z.

interfaces strongly affect the orientation of the permanent and induced dipoles. Moreover, the nearly unchanged form of the distribution lead us to believe that surface effects on the orientation will continue much further from the interface than we can probe in these simulations. These long-range effects on molecular orientation have recently been studied experimentally by Teschke and de Souza[29] in their atomic force microscopy (AFM) study of the gas-liquid interface. They show that AFM tips detect attractive forces at distances as far as 250 nm and attributed the phenomena to the broken hydrogen bonds at the interface. After $z\approx-12$ Å, i.e., in the interfacial region, the distributions show a narrower Gaussian distribution with a peak larger than that observed in the bulklike liquid region. The distribution with the largest peak occurs at $z\approx-15.5$ Å for both permanent and induced dipoles, and from this point the peak of the distributions decreases in magnitude. At $z\approx-21$ Å the peak is almost zero because the small number of the molecules present in this slab. The maximum value of the peak for the induced dipole orientation keeps a preferred value of 0°, while for the permanent dipoles the preferred orientation deviates to 10°, as indicated by the heavy lines in Figs. 3 and 4. The larger peaks in this region correspond to an increase in the number of molecules with induced dipoles parallel to the interface. A similar behavior of dipole orientation was observed by Motakabbir and Berkowitz in their simulation of liquid water using the TIP4P model.[12]

Permanent dipoles have constant magnitude since their molecular geometry is fixed. Induced dipoles may vary in both magnitude ($\mu_j=|\mathbf{p}_j|$) and orientation with respect to the internal coordinates. The distributions of the magnitude of the induced dipole as a function of z are shown in Fig. 5, with the average value of each distribution shown by the heavy line. The distributions are Gaussian. From the center of the bulklike region up to slabs located at $z\approx-12$ Å, the distributions are unchanged and the peaks have mean and deviation average values of 0.878 ± 0.005 D. In this region, the permanent and induced dipoles have identical orientation distributions; therefore, their magnitudes can be simply added producing a total value of 2.733 ± 0.005 D in agreement with the reported value in reference.[9] After $z\approx-12$ Å, i.e., in the interfacial region, the magnitude of the peaks in the histograms decreases monotonically and at $z\approx-21$ Å the peaks are almost zero. The average value of the magnitude of the induced dipole also decreases monotonically in this region, reaching a value of $\mu\approx0.33$ D at $z\approx-21$ Å; the decrease is likely due to the fact that molecules in the interface interact with fewer molecules than those in the bulklike region, and then produce a smaller induced dipole magnitude. In the simulations of Motakabbir and Berkowitz[12] using the TIP4P polarizable model of water, a similar behavior of μ at the interface was observed. They found that μ decreased monotonically in magnitude to $\mu\approx0.37$ D and the alignment with the permanent dipoles decreased.

B. Surface tension

In order to evaluate the influence of polarizability on the interfacial forces involved in γ, we evaluate the difference between the normal and tangential pressure profiles, $P_N(z)-P_T(z)$, and integrate those profiles to obtain the respective contribution to γ. $P_N(z)$ and $P_T(z)$ were calculated for the permanent-permanent (PePe), induced-induced (InIn), permanent-induced (PeIn) dipoles, and (exp-6) interactions using Eqs. (11)–(15). We plot $P_N(z)-P_T(z)$ for each contribution in Figs. 6–8. The sum of all those contributions is also plotted in Fig. 8. The contribution to γ according to Eq. (9) is also plotted in each figure. We discuss each of the contributions in the following.

The PePe pressure-difference profile can be decomposed into the sum of three contributions, which correspond to the electrostatic interactions due to the fixed Gaussian distributed charges of the permanent dipoles; in Fig. 6(a) we plot $P_N(z)-P_T(z)$ arising from oxygen-oxygen, hydrogen-hydrogen, and oxygen-hydrogen, interactions. Intermolecular interactions between oxygen-oxygen and hydrogen-hydrogen atoms have a negative contribution to the PePe profile, while those of the oxygen-hydrogen atoms have a positive contribution. This is simply attributable to the fact that like charges have repulsive interactions, while opposite charges have at-

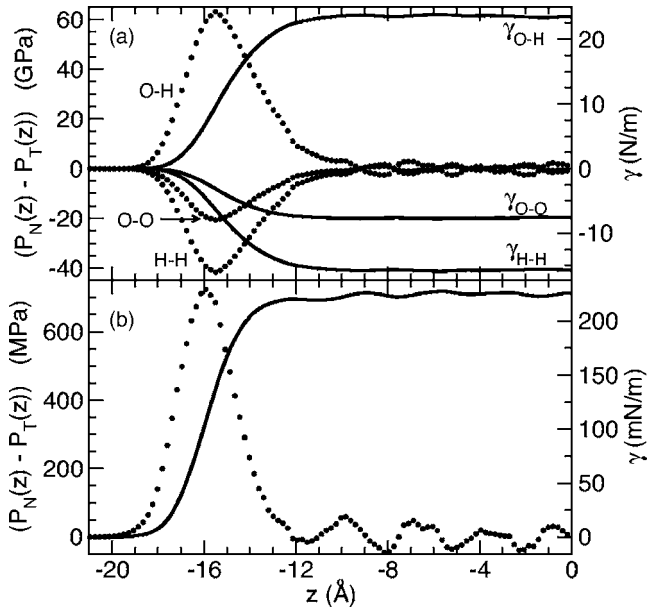

FIG. 6. (a) $P_N(z)-P_T(z)$ is shown in the left axis. Circles represent the profile of the differences between the normal and tangential pressures due to Gaussian distributed charge interactions. γ is shown in the right axis. Continuous lines represent the profiles of γ. (b) Axes are the same as (a). Circles represent the profile of the differences between the normal and tangential pressures due to the net contribution of Gaussian distributed charges interactions. Continuous line represents the profile of γ.

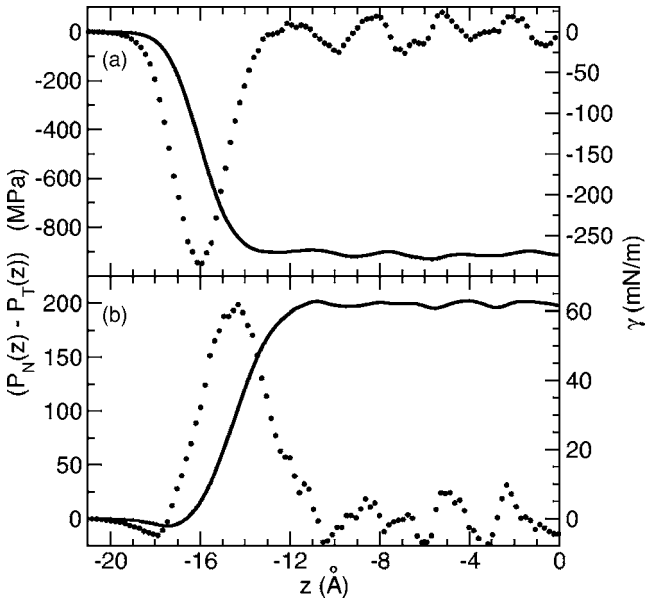

FIG. 8. (a) $P_N(z)-P_T(z)$ is shown in the left axis. Circles represent the profile of the differences between the normal and tangential pressures due to (exp-6) interactions. γ is shown in the right axis. Continuous lines represent the profiles of γ. (b) Axes are the same as (a). Circles represent the profile of the differences between the normal and tangential pressures due to the sum of all the intermolecular interactions. Continuous line represents the profile of γ.

tractive interactions. The difference in pressures produces well-defined peaks at $z \approx -15.5$ Å with magnitudes of ≈ 63.0, -41.7, and -20.8 GPa for the oxygen-hydrogen, hydrogen-hydrogen, and oxygen-oxygen interactions, respectively. In terms of the physical meaning of γ, a total positive value means that if we want to create tangential area at the interface, we need to apply a tangential surface force to the interface big enough to overcome γ. A total negative value means that the system does not exhibit cohesive surface forces and hence an interfacial region will not develop, and such a system will not have a defined liquid state. As shown in Fig. 6(b), when we sum each of the individual contributions from the fixed charges, the total contribution to $\gamma = 0.22$ N/m, around two orders of magnitude lower than its corresponding contributions. Thus the individual positive and negative contributions nearly cancel each other.

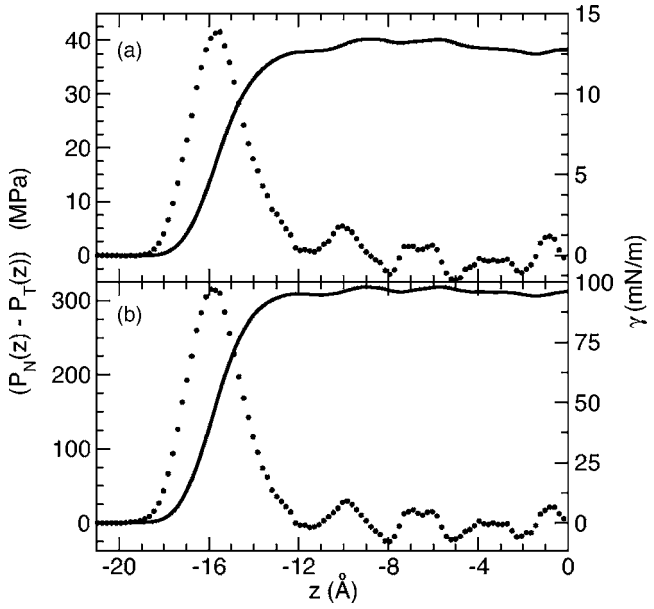

FIG. 7. (a) $P_N(z)-P_T(z)$ is shown in the left axis. Circles represent the profile of the differences between the normal and tangential pressures due to induced-induced dipole interactions. γ is shown in the right axis. Continuous lines represent the profiles of γ. (b) Axes are the same as (a). Circles represent the profile of the differences between the normal and tangential pressures due to permanent-induced dipole interactions. Continuous line represents the profile of γ.

The interactions of the induced dipoles (InIn and PeIn) cannot be directly attributed to the atomic components since the induced dipolar interactions are calculated from vectors located at the molecules' center of mass. Figure 7(a) shows $P_N(z)-P_T(z)$ for the InIn interactions, which produce a well-defined peak with differences in the pressure of up to 41 MPa and a small positive contribution to γ of 12.71 mN/m. We point out that while the magnitude of the induced dipoles represent approximately one third of the total value of the dipole in the bulklike region, the contribution from the pure induced interactions to γ is only $\approx 1/18$ of the contribution from pure permanent dipole interactions. This relatively small contribution from the pure induced dipoles is due to the fact that the interactions contributing to γ are from molecules at the interface. The average magnitude of the induced dipoles of the interfacial molecules decreases monotonically from the mean value in the bulklike region of 0.878 D down to values close to 0.33 D (Fig. 5). The calculation of γ uses the normal and tangential pressure definitions, which is proportional to the square of the magnitude of the dipoles. If we consider the limit in which all the molecules at the interface keep the mean bulklike value of 0.878 D for induced dipoles, then the induced dipoles would

TABLE I. Contributions to γ due to electrostatic and dispersion interactions. Numbers in parenthesis are approximate error bars, discussed in text.

Interaction	γ (mN/m)
Permanent-permanent dipoles	224.01
Induced-induced dipoles	12.71
Permanent-induced dipoles	96.22
Exp-6 interactions	−271.52
Long-range correction (Eq. (16))	7.23 (±0.30)
Total	68.65 (±0.30)

have a contribution to $\gamma \approx 1/4$ of that due to the permanent dipoles. The other limit, where all the molecules have the surface value of induced dipoles with magnitude of 0.33 D, would produce an induced dipole contribution to $\gamma \approx 1/32$ of that due to the permanent dipoles. The value obtained from the simulation of 1/18 falls between these two limits, and hence the small contribution of the induced dipoles to γ is mostly due to the monotonic change in the average magnitude of the induced dipoles at the interface. Interactions between PeIn dipoles are shown in Fig. 7(b) and the difference in pressures shows a well-defined peak (320 MPa). The integration of this profile results in a net contribution to γ of 96.22 mN/m, larger than the InIn contribution, but still less than half of that due to PePe contribution.

Lastly we examine the contribution from the dispersion interactions in Fig. 8(a), which have a negative difference between the normal and tangential pressures. The difference has a peak with a minimum at −960 MPa. This negative profile produces a negative contribution to γ of −271.52 mN/m. The sign of the contribution to γ is due to the fact that the mean oxygen-oxygen distance is smaller than the parameter σ, which represents the distance where the core exponential potential becomes repulsive, and hence would generate a negative contribution to γ. Oxygen atoms are closer than σ due to the strong electrostatic attraction between oxygens and hydrogens.

The contribution of each interaction is tabulated in Table I, along with the contribution due to long-range attractive interactions calculated using Eqs. (16) and (17). Summing all contributions, we find the total value of $\gamma = 68.65$ mN/m for liquid water at 298.15 K. The large fluctuation in the various contributions relative to the sum is an indicator of the difficulty to obtain reliable data. The uncertainty in the long-range correction to γ [Eq. (16)] is due to the uncertainty of the liquid density used in Eqs. (16) and (17). Figure 8(b) shows the total pressure-difference profile, which shows a well-defined peak of 200 MPa. While the peaks of the pressure-difference profile of the contributions are located at $z \approx -16$ Å, the peak of the total pressure-difference profile is located at $z \approx -13.5$ Å, showing that most of the cancellation among the contributions occurs after $z \approx -13.5$ Å. The total pressure-difference profile also shows an additional feature at $z \approx -18$ Å, where a small negative peak develops with a minimum of ≈−14 MPa. The fact that we have two peaks probably indicates that at the interface we have two opposite surface forces acting at different distances from the center of the slab. The surface force close to the bulklike region is large and cohesive while the surface force close to the vacuum is small and uncohesive. After integration and inclusion of the long-range correction, the total value of $\gamma = 68.73$ mN/m, which matches the sum of individual values, as we would expect. The total computed values agree with the experimental value within a relative error of ≈4%.[30]

IV. CONCLUSIONS

Liquid water in vacuum was simulated using a polarizable model with fixed Gaussian distributed charges at 298.15 K via MD. The simulations produced a condensed liquid phase with an average density that agrees well with the experimental value and with other calculations for the model using GEMC.

Due to the small size of the simulated system, the two interfaces affect the behavior of the molecules through the entire slab. This effect is more pronounced for the distribution of molecular orientations, which is strongly biased to be parallel to the interface, even at the center of the slab. Therefore the simulated system does not have a truly bulk region where molecules are unaffected by the interface, even though the liquid slab extended across 31 Å, which is more than three times the cutoff radius of the interactions. At the bulklike region, induced dipoles have the same orientation distributions as permanent dipoles with uniform average magnitude, while at the interface the average magnitude decreases monotonically, capturing the transition in the induced dipoles between molecules at the liquid phase and isolated molecules in the vacuum. At the interface the number of molecules with induced dipoles parallel to the interfaces increases, while the permanent dipoles showed a preference to be located at angles 10° from the interface.

We examined the five contributions to γ corresponding to the permanent-permanent, induced-induced, permanent-induced dipoles, short, and long range dispersion interactions. All the dipole interactions have a net positive contribution to γ and the permanent-permanent dipole interaction is the result of three contributions due to fixed Gaussian charges interactions that almost cancel each other to produce a net contribution to γ two orders of magnitude lower than its constitutive parts. Short ranged dispersion interactions produced a negative contribution to γ due to the fact that the oxygen-oxygen separation is in the repulsive core, while the long-range dispersion interactions has a positive contribution. From the total pressure-difference profile, we find that there are two surface forces acting at the interface, one large and positive surface force acting close to the bulklike region and another small and negative acting close to the vacuum. This result is not unique to water, having also been observed in Lennard-Jones systems.[31]

Based on our work, the contribution from polarizability to the surface forces is important for this model because polarizability contributions represent around one third of the total positive contributions. While we cannot compare the individual contributions to γ with experiments, our overall value is consistent with experiments. More experimental information about the structure of water at the interface is needed to validate the other properties reported here.

Future work will systematically study the effect of the thickness of the liquid slab in the orientation and development of bulk liquid phases. The effect of temperature in γ for vapor-liquid and liquid-liquid equilibria will be also evaluated with this promising model. Additionally, an investigation of both surface effects and polarizability on the known anomalous thermodynamic[2,32] and dynamic[33] properties of bulk water would be valuable. It would also be interesting to determine the surface tension with the test-area technique recently developed by Gloor *et al.*[34]

ACKNOWLEDGMENTS

We thank the U. S. Department of Energy and the National Science Foundation for support under Grant No. DMR-0427239. We also thank Universidad Michoacana de San Nicolás de Hidalgo (México) and CONACYT (México) for support under Grant No. 48568.

[1] P. G. Debenedetti, J. Phys.: Condens. Matter **15**, R1669 (2003).
[2] P. G. Debenedetti and H. E. Stanley, Phys. Today **566**(6), 40 (2003).
[3] C. A. Angell, Annu. Rev. Phys. Chem. **55**, 559 (2004).
[4] J. M. Prausnitz, R. N. Lichtenthaler, and E. Gomes de Azevedo, *Molecular Thermodynamics of Fluid Phase Equilibria*, 3rd ed. (Prentice Hall, Englewood Cliffs, New Jersey, 1998).
[5] C. Wohlfarth and B. Wohlfarth, *Surface Tension of Pure Liquids and Binary Liquid Mixtures* (Springer, Berlin, 1997).
[6] M. L. Schlossman, Physica B **357**, 98 (2005).
[7] A. Braslau, P. S. Pershan, G. Swislow, B. M. Ocko, and J. Als-Nielsen, Phys. Rev. A **38**, 2457 (1988).
[8] J. L. Rivera, M. Predota, A. A. Chialvo, and P. T. Cummings, Chem. Phys. Lett. **357**, 189 (2002).
[9] P. Paricaud, M. Predota, A. A. Chiavo, and P. T. Cummings, J. Chem. Phys. **122**, 244511 (2005).
[10] P. Jedlovszky and R. Vallauri, J. Chem. Phys. **122**, 081101 (2005).
[11] K. Kiyohara, K. E. Gubbins, and A. Z. Panagioutopoulos, Mol. Phys. **94**, 803 (1998).
[12] K. A. Motakabbir and M. L. Berkowitz, Chem. Phys. Lett. **176**, 61 (1991).
[13] P. Liu, E. Harder, and B. J. Berne, J. Phys. Chem. B **109**, 2949 (2005).
[14] T. R. Dyke and J. S. Muenter, J. Chem. Phys. **59**, 3125 (1973).
[15] W. S. Benedict, N. Gailar, and E. K. Plyler, J. Chem. Phys. **24**, 1139 (1956).
[16] M. P. Allen and D. J. Tildesley, *Computer Simulations of Liquids* (Clarendon, Oxford, 1987).
[17] S. Patel and C. L. Brooks, J. Chem. Phys. **123**, 164502 (2005).
[18] F. M. Juarez-Guerra, J. L. Rivera, A. Zuniga-Moreno, L. A. Galicia-Luna, J. L. Rico, and J. Lara, Sep. Sci. Technol. **41**, 261 (2006).
[19] A. E. Ismail, G. S. Grest, and M. J. Stevens, J. Chem. Phys. **125**, 014702 (2006).
[20] F. Goujon, P. Malfreyt, J. M. Simon, A. Boutin, B. Rousseau, and A. H. Fuchs, J. Chem. Phys. **121**, 12559 (2004).
[21] J. L. Rivera and J. Alejandre, Colloids Surf., A **207**, 223 (2002).
[22] H. A. Patel, E. B. Nauman, and S. Garde, J. Chem. Phys. **119**, 9199 (2003).
[23] S. S. Jang, S. T. Lin, P. K. Maiti, M. Blanco, W. A. Goddard, P. Shuler, and Y. C. Tang, J. Phys. Chem. B **108**, 12130 (2004).
[24] W. G. Hoover, A. J. C. Ladd, and B. Moran, Phys. Rev. Lett. **48**, 1818 (1982).
[25] D. J. Evans and G. P. Morris, Phys. Lett. **98**, 433 (1983).
[26] D. J. Evans and S. Murad, Mol. Phys. **34**, 327 (1977).
[27] J. Alejandre, D. J. Tildesley, and G. A. Chapela, Mol. Phys. **85**, 651 (1995).
[28] S. Ozeki, Langmuir **5**, 181 (1989).
[29] O. Teschke and E. F. de Sousa, Phys. Chem. Chem. Phys. **7**, 3856 (2005).
[30] N. B. Vargaftik, V. N. Volkov, and L. D. Voljak, J. Phys. Chem. Ref. Data **12**, 817 (1983).
[31] A. Trokhymchuk and J. Alejandre, J. Chem. Phys. **111**, 8510 (1999).
[32] O. Mishima and H. E. Stanley, Nature (London) **396**, 329 (1998).
[33] F. W. Starr, F. Sciortino, and H. E. Stanley, Phys. Rev. E **60**, 6757 (1999).
[34] G. J. Gloor, G. Jackson, F. J. Blas, and E. de Miguel, J. Chem. Phys. **123**, 134703 (2005).
[35] L. Haar, J. S. Gallagher, and G. S. Kell, *NBS/NRC Steam Tables* (Hemisphere, Washington, DC, 1984).